Contrib Mineral Petrol (2000) 139: 470–484

Cin-Ty Lee · Roberta L. Rudnick
William F. McDonough · Ingo Horn

Petrologic and geochemical investigation of carbonates in peridotite xenoliths from northeastern Tanzania

Received: 30 July 1999 / Accepted: 5 February 2000

Abstract Primary carbonates in peridotite xenoliths from the East African Rift in northeastern Tanzania occur as intergranular patches with accessory minerals (olivine and spinel), as patches with accessory magmatic minerals (nepheline), and as round monomineralic inclusions in primary olivine grains. All are characterized by calcitic compositions (Ca/Ca + Mg + Fe from 0.83 to 0.99), extremely low SiO_2 + Al_2O_3 + Na_2O + K_2O, low trace element abundance [total rare-earth element (REE) abundance <25 ppm], uniform extinction, and lack of reaction textures with the host xenolith. Calculated Fe–Mg exchange coefficients between carbonate and primary olivine indicate disequilibrium in most samples. Combined with the lack of significant reaction textures, this suggests that the carbonates were introduced shortly before or during eruption of the host magma. A global compilation of electron microprobe analyses of mantle-derived carbonates (in xenoliths, xenocrysts, and megacrysts) reveals compositional clusters near end member calcite, end member magnesite, and stoichiometric dolomite. Eutectic liquid compositions are less common, suggesting that many carbonate inclusions reported worldwide may be crystalline precipitates. Likewise, the calcites in this study are not interpreted to represent quenched carbonatitic melts, but are interpreted instead to be crystalline cumulates from such melts. These inferences are consistent with recent experiments, which show that carbonatitic melts cannot become more calcitic than $CaCO_3$~80 wt%. Low trace element abundance may be a diagnostic feature of cumulate carbonate, and in combination with petrography and major element composition, serve to distinguish it from quenched carbonated liquid.

C.-T. Lee (✉) · R. L. Rudnick · W. F. McDonough · I. Horn
Department of Earth and Planetary Sciences,
Harvard University, 20 Oxford St., Cambridge,
MA 02138, USA
e-mail: ctlee@eps.harvard.edu
Tel.: +1-617-484-2397; Fax: +1-617-496-0434

Present Address:
Lab for Inorganic Chemistry, ETH Zürich,
University St. 6, CH-8092, Zürich, Switzerland

Editorial responsibility: T. L. Grove

Introduction

Although primary, mantle-derived carbonates are rare in mantle-derived rocks (Canil 1990), there are increasing reports of occurrences from around the world and from diverse tectonic environments (McGetchin and Besancon 1973; Hunter and Smith 1981; Berg 1986; Amundsen 1987; Bulanova and Pavlova 1987; Smith 1987; Ionov et al. 1993; Yang et al. 1993; Frezzotti et al. 1994; McInnes and Cameron 1994; Pyle and Haggerty 1994; Schiano et al. 1994; Zhang and Liou 1994; Kogarko et al. 1995; Ionov et al. 1996; Ionov 1998; Norman and Pearson 1998; Saal et al. 1998). These carbonates potentially provide insights into the origin of carbonatite melts and mantle metasomatism and to the problem of determining where and in what form carbon is stored in the mantle (Barker 1996). For instance, if these carbonates are quenched liquids, then their compositions can be used to determine whether carbonatite lavas are (1) primary mantle melts, (2) primary melts modified by wall-rock interaction, or (3) products of crystal fractionation or carbonate–silicate liquid immiscibility (e.g., Wallace and Green 1988; Dalton and Wood 1993a; W.-J. Lee and Wyllie 1998; Wyllie and W.-J. Lee 1998). Additionally, experiments suggest that carbonatitic melts have low viscosities and low wetting angles (Minarik and Watson 1995; Dobson et al. 1996). Thus, by analogy with carbonatitic lavas, which are highly enriched in incompatible elements, carbonate melts are prime candidates for metasomatic agents in the lithospheric mantle (Meen 1987; Green and Wallace 1988; Yaxley et al. 1991; Dautria et al. 1992; Dalton and Wood 1993a; Hauri et al. 1993; Rudnick et al. 1993; Yaxley and Green 1996; Wiechert et al. 1997; Yaxley et al. 1998; Coltorti et al.

1999). In contrast, if the carbonates are crystal cumulates, as in the case of primary mantle carbonates or precipitates from a carbonate melt, their bulk compositions are not identical to those of carbonatitic melts.

There is an ongoing debate over whether natural carbonate inclusions are crystalline precipitates or quenched liquids (W.-J. Lee et al. 1994). On one hand, certain textural features, such as curved menisci and globular shapes, have been interpreted as evidence for quenched liquids (e.g., Amundsen 1987; Pyle and Haggerty 1994; Kogarko et al. 1995; Norman and Pearson 1998). On the other hand, recent experiments, such as those of W.-J. Lee and Wyllie (1996, 1998), indicate that carbonatitic melts cannot have $CaCO_3 >$ 80 wt%, regardless of whether they are primary melts, immiscible liquids, or highly evolved melts. Because most carbonate inclusions in peridotite xenoliths are calcitic, these authors are of the opinion that most, if not all, carbonates in mantle xenoliths are cumulates. Likewise, Ionov (1998) has argued on the basis of textural and major element data that globular carbonates may be crystal cumulates.

To shed light on this debate, we combine petrography with whole-rock and *in situ* trace element analyses and stable isotopic analyses to arrive at an independent interpretation of the nature of these carbonates. We assume that quenched carbonate melts should have high contents of incompatible trace elements, analogous to natural carbonatitic lavas (Woolley and Kempe 1989). Crystalline calcite excludes most incompatible trace elements from its lattice (Law et al. 1999), a behavior consistent with the fact that carbonate minerals from carbonatites tend to have slightly to significantly lower trace element contents than the bulk rock (e.g., Keller and Spettel 1995). Ionov (1998) showed that carbonates in Spitsbergen and Mongolian xenoliths have extremely low trace element contents, arguing that such carbonates are not quenched liquids, but crystal cumulates.

The xenolith suites

Carbonate-bearing peridotites were collected from several xenolith localities in the East African Rift: Labait, Pello, Eledoi, and Monduli volcanoes (see Dawson 1992 for locations). These represent the first carbonate-bearing xenoliths described from East Africa.

The Pleistocene Labait volcano is located on the northeastern edge of the Tanzanian craton, just south of Mount Hanang. The volcano consists of an olivine–melilitite lava, a tuff, and a carbonatite. The olivine–melilitite consists of zoned olivine phenocrysts and zoned, low Cr clinopyroxene megacrysts set within a matrix of microphenocrysts of olivine (Fo_{84}), Ti-augite, Ti-magnetite, perovskite, intergranular nepheline, and melilitite (Dawson et al. 1997). The xenolith suite consists of chromite and garnet harzburgites, garnet lherzolites, dunites, pyroxenites, and abundant Fe-rich dunites (Dawson et al. 1997; Chesley et al. 1999; Dawson 1999; C.-T. Lee and Rudnick 1999). The Fe-rich dunites make up 75% of the xenolith population. Carbonates were found in only 2 out of over 50 thin sections examined: a Fe-rich wehrlite (LB58) and an Fe-rich phlogopite-bearing dunite (LB19) (Table 1). The maximum pressures recorded by garnet-bearing xenoliths range up 4.9 GPa (Dawson et al. 1997; C.-T. Lee and Rudnick 1999), indicating that the lithosphere beneath Labait extends to depths of about 150 km.

Pello Hill and Eledoi are side-by-side Quaternary tuff cones and craters, located in the rift valley proper in northern Tanzania (Dawson and Smith 1988). These sites are near the well-known carbonatite volcanoes, Ol Doinyo Lengai and Kerimasai. The host lava for both Pello and Eledoi are fine-grained red scoria, with bulk-rock chemistry akin to olivine–melilitites and olivine–

Table 1 Petrographic summary

Sample	Host rock	Carbonates	Fig.
Primary carbonates			
Monduli			
MON7, MON5	Clinopyroxene-free spinel harzburgite	Interstitial calcite associated with tiny euhedral grains of highly forsteritic olivine (up to Fo_{95}) and tiny apple-green spinels; calcites exhibit uniform extinction and good cleavage	1A
MON5p	Olivine phenocryst in basalt	Round monomineralic calcite inclusions in olivine phenocrysts within host basalt; one inclusion is associated with a melt patch	1C
MON5r	Host lava	Monomineralic calcite patches abound in the host basalt; most have feathery or resorbed rims	–
Labait			
LB58	Chromite-bearing Fe-rich wehrlite	Interstitial calcite associated with tiny nepheline, but otherwise monomineralic	1B
Eledoi			
EL14	Fe-rich dunite	Round monomineralic calcite inclusions in groundmass olivines	1E, F
Carbonates of hydrothermal origin?			
Labait			
LB19	Fe-rich dunite (minor clinopyroxene)	Monomineralic interstitial calcite; no associated mineralogy and no reaction textures	1H
Eledoi			
EL10	Spinel harzburgite	Zeolite-bearing calcite patches; occurs interstitially and as fractures crosscutting entire xenolith and through primary mineralogy	1G
Pello hill			
PEL2	Spinel harzburgite	Zeolite-bearing calcite patches; occurs interstitially and as fractures crosscutting entire xenolith and through primary mineralogy	1D

nephelinites (Dawson and Smith 1988). Xenoliths are abundant at both localities and consist of rounded to subangular blocks of extremely fresh spinel lherzolite, harzburgite, and dunite up to 30 cm across. Many of the xenoliths are characterized by extensive veins, consisting of amphibole, phlogopite, diopside, ilmenite, rutile, and sulfide. Preliminary investigations have so far revealed three carbonate-bearing xenoliths (PEL2, EL10, EL14; lithologic descriptions are given in Table 1). Based on the absence of garnet-bearing lithologies, the lithosphere beneath this region probably extends no deeper than 90 km, consistent with geophysical constraints, which place lithospheric thickness beneath the rift valley at approximately 90 km (Ebinger et al. 1997).

Monduli volcano, located in the southern portion of the rift valley, is probably Quaternary, based on K–Ar ages between 1.7 and 2.2 Ma for nearby volcanics (Evans et al. 1971; MacIntyre et al. 1974). The lava consists of phenocrysts of olivine, augite, and magnetite, and feathery blebs of calcite. Xenoliths are sparse, occurring locally in lava flows on the northwestern side of the volcano and are dominated by spinel harzburgites (MON5 and MON7 in Table 1). Garnet-bearing lithologies have not yet been observed in the tens of xenoliths examined at this site. Carbonates occur in four out of seven thin sections in our collection.

Results

Petrography of carbonates

Photomicrographs of representative carbonates are shown in Fig. 1. Mineralogies of the carbonate-bearing xenoliths and morphologies of the carbonates are given in Table 1. Representative mineral chemistries for primary and carbonate-related minerals assemblages are given in Table 2.

Calcite–olivine intergrowths

Carbonate occurs as intergranular patches up to 2 mm in diameter, typically surrounding primary peridotitic chromite ($Cr/Cr + Al = 0.58$) in the clinopyroxene-free harzburgites from Monduli (MON7; Fig. 1A). In some samples, the patches are connected to each other by carbonate veins, following grain boundaries or filling fractures. Fluid inclusions are abundant in healed fractures cross-cutting primary olivines. Associated with the carbonate patches are secondary olivines and spinels, the former occurring as small (< 50 μm) euhedral grains "floating" within the carbonate, and the latter occurring abundantly as tiny (< 6 μm) euhedral grains embedded in the carbonate rim. The secondary spinels differ from primary spinels in the harzburgite by appearing pale green rather than dark brown in plane-polarized light. The secondary olivines differ from primary olivines by being more magnesian (up to Fo_{95}) and having variable, often low NiO contents (0.2–0.3 wt%). As a result, they lie distinctly off the trend of primary peridotitic olivines in an MgO–NiO plot (Fig. 2). Overall, the association of magnesian olivine with carbonate resembles other reported occurrences of olivine–carbonate intergrowths in peridotite (Ionov et al. 1993; Kogarko et al. 1995). However, in our samples, there is no evidence for the pervasive replacement of orthopyroxene by clinopyroxene, so commonly observed in carbonatite-metasomatized rocks (Meen 1987; Green and Wallace 1988; Yaxley et al. 1991; Dautria et al. 1992; Dalton and Wood 1993a; Hauri et al. 1993; Ionov et al. 1996; Yaxley et al. 1998; Coltorti et al. 1999).

Carbonate + nepheline

In LB58, a chromite-bearing Fe-rich wehrlite, intergranular patches (< 500 μm) of coexisting carbonate and nepheline (50–100 μm) occur in thin section (Fig. 1B). These patches mantle primary chromites, but there appears to be no reaction with the peridotitic wallrock or primary chromites. This sample also contains vugs, which may have formerly been occupied by carbonates that were "plucked out" during thin section preparation.

Inclusions in phenocrystic and peridotitic olivines

Carbonates fully enclosed in primary minerals, such as olivine, occur in EL14, a veined Fe-rich dunite xenolith (Fig. 1E, F). These carbonates are perfectly round (< 50 μm). Round holes scattered throughout this sample may have also been occupied by carbonates. Only one fully enclosed carbonate inclusion was found in olivine in PEL2, a spinel harzburgite. Fractures extending from the carbonate inclusion to the exterior of the host mineral are rare. Overall, these inclusions resemble those found in pyropic and eclogitic garnet xenocrysts in Colorado Plateau kimberlites (McGetchin and Besancon 1973; Hunter and Smith 1981; Smith 1987).

Two carbonate inclusions (< 1.5 mm) were found within a large olivine phenocryst (MON5p) in the lava rind of a Monduli xenolith (Fig. 1C). One inclusion is monomineralic, whereas the other consists of a round carbonate globule coexisting with an aphyric lava whose mineralogy is similar to that of the host basalt.

Carbonates in host lava

Carbonates also occur as discrete grains in the host lava (primarily at Monduli) up to 4 mm in size. These may be xenocrystic because they have highly resorbed rims and feathery textures. Their major element compositions are not different from those within the peridotites.

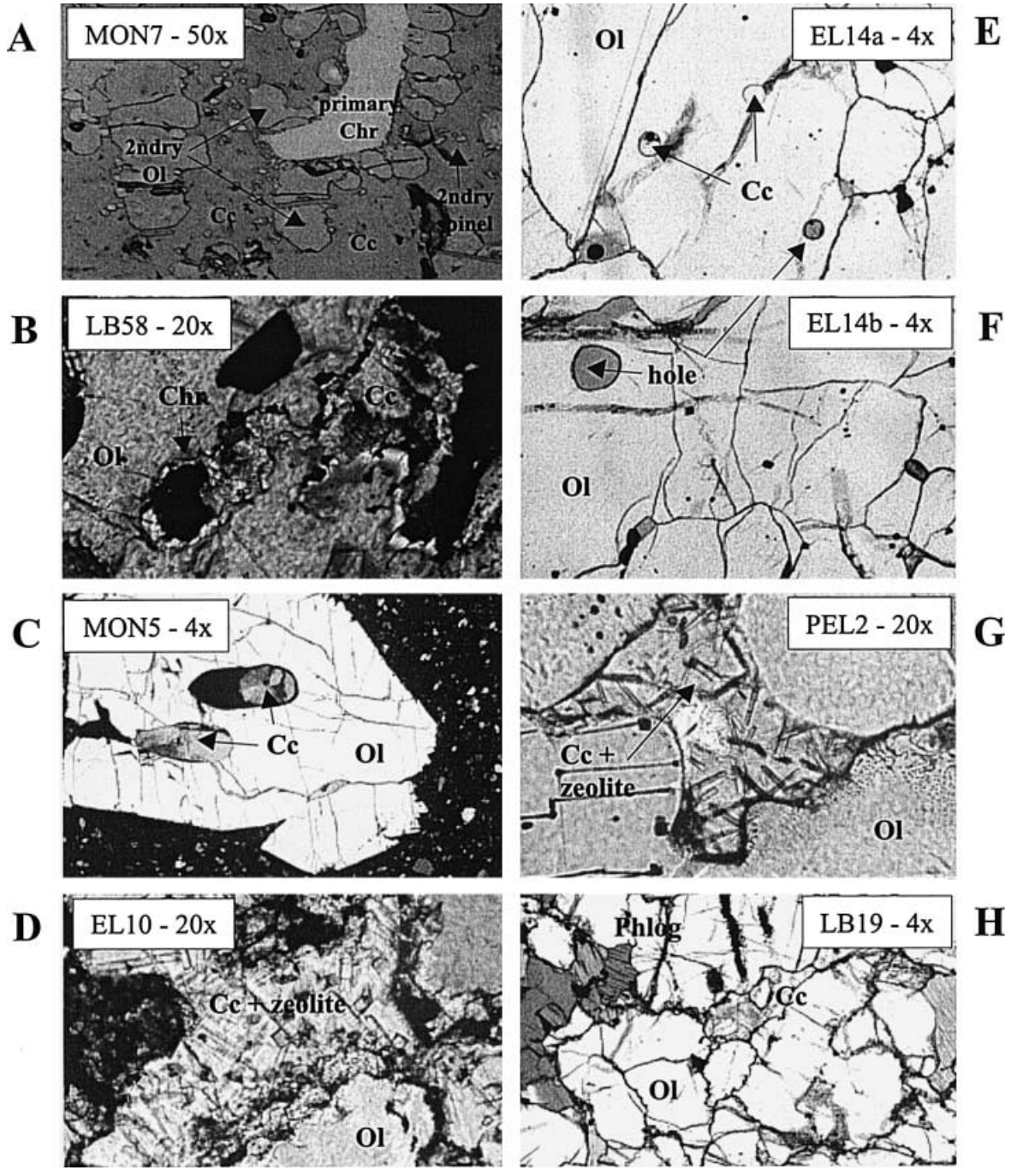

Fig. 1 Photomicrographs of representative carbonate inclusions. MON7, EL14, LB58, and MON5 are believed to be primary, in the sense that they are not related to surficial weathering or hydrothermal alteration. PEL2 and EL10 contain zeolites and are interpreted to have originated from hydrothermal alteration. LB19 has insufficient textural and mineralogic features to assess whether it is primary or secondary. Straight lines in lower left corner of PEL2 panel are probe tracks in epoxy. LB58, MON5, and EL10 are in crossed polars; remaining panels are in plane light. Petrographic and lithologic descriptions given in Table 1

Hydrothermal carbonates (carbonate ± zeolite)

Carbonate in two harzburgites (PEL2 and EL10) contain acicular crystals of K–Ca–Na-bearing zeolites (~60 μm long, < 6 μm in diameter). In PEL2, the carbonate–zeolite intergrowths occur as intergranular patches (< 500 μm) (Fig. 1G). In EL10, the intergrowths fill a planar crack, which crosscuts the entire xenolith (Fig. 1D). These intergrowths undoubtedly originate from hydrothermal alteration during or shortly after eruption.

Featureless carbonate patches (< 750 μm) occur in LB19, an Fe-rich dunite. These patches consist of large, interlocking domains of carbonate, but are otherwise nondescript (Fig. 1H). As will be discussed later, the featureless character of these carbonates makes it difficult to assess whether they are primary or secondary.

Table 2 Representative electron microprobe analyses of mineral phases. *OL* Olivine, *CHRMT* chromite, *PHLOG* phlogopite, *CC* carbonate, *OPX* orthopyroxene, *CPX* clinopyroxene, *ILM* ilmenite, *AMPH* amphibole, *NEPH* nepheline

	Monduli silicate phases									Monduli carbonate phases							
	Primary assemblage			OL in carbonate patches			Phenocrysts in lava			In lava		In OL phenocryst		Inclusions in xenoliths			
	OL	OPX	CHRMT				OL	CPX	ILM	3B	6B	5-A	5-B	MON3	MON5	MON6	MON7
SiO_2	40.59	56.21	0.10	40.75	40.67	40.75	39.58	42.08	0.11	–	–	0.17	–	–	0.14	–	–
TiO_2	0.00	0.01	0.07	0.01	0.00	0.01	0.01	2.87	19.05	–	–	–	–	–	–	–	–
Al_2O_3	0.01	1.48	22.74	0.09	0.04	0.09	0.04	5.95	4.29	–	–	–	–	–	–	–	–
Cr_2O_3	0.02	0.34	47.23	0.20	0.21	0.20	0.05	0.23	0.18	–	–	–	–	–	–	–	–
V_2O_5	–	–	0.18	–	–	–	–	–	0.46	–	–	–	–	–	–	–	–
FeO	6.54	4.21	12.24	4.98	6.23	4.98	13.21	7.52	67.73	0.01	0.62	0.08	1.34	0.07	0.10	1.66	0.10
MnO	0.11	0.10	0.13	0.08	0.09	0.08	0.18	0.13	0.47	0.00	0.65	0.39	0.33	0.01	0.21	0.96	0.03
MgO	51.29	36.22	17.33	52.05	51.53	52.05	46.32	12.73	5.86	2.27	0.85	0.71	1.03	2.69	1.00	1.77	0.51
NiO	0.42	–	0.15	0.37	0.22	0.37	0.35	–	0.02	–	–	–	–	–	–	–	–
CaO	0.03	0.24	0.03	0.17	0.02	0.17	0.20	22.22	0.10	53.50	53.35	54.19	51.39	52.98	54.33	51.67	55.27
Na_2O	–	0.07	–	–	–	–	–	0.57	–	–	–	0.07	–	–	0.07	–	–
SrO	–	–	–	–	–	–	–	–	–	0.04	0.07	0.05	0.10	0.05	0.08	0.06	0.07
K_2O	–	–	–	–	–	–	–	–	–	–	–	0.01	–	–	0.01	–	–
F	–	–	–	–	–	–	–	–	–	–	–	–	–	–	–	–	–
Cl	–	–	–	–	–	–	–	–	–	–	–	–	–	–	–	–	–
Total	99.01	98.88	100.21	98.70	98.99	98.70	99.94	94.30	98.27	55.82	55.54	55.67	54.19	55.80	55.94	56.12	55.98
Mg/(Mg + Fe)	0.93	0.94	0.72	0.95	0.94	0.95	0.86	0.75	0.13	1.00	0.71	0.94	0.58	0.99	0.95	0.66	0.90
Ca/(Ca + Mg + Fe)	–	–	–	–	-	–	–	–	–	0.94	0.97	0.98	0.95	0.93	0.97	0.93	0.99

Table 2 (Contd.)

	Labait 58 (LB58)						Eledoi 14 (EL14)								
	Primary assemblage				In carbonate		OL	OL By vein	CPX In vein	CHRMT	CHRMT In vein	ILM In vein	AMPH In vein	PHLOG	CC
	OL	CPX	CHRMT	PHLG	CC	NEPH									
SiO_2	39.93	51.35	0.03	39.81	0.03	42.69	39.23	39.06	52.23	0.05	0.07	0.03	42.88	37.83	1.02
TiO_2	0.00	1.37	1.08	5.81	–	0.14	0.01	0.03	1	7.65	9.43	51.76	3.61	4.29	–
Al_2O_3	0.01	2.04	16.10	11.18	–	31.76	0.01	0.01	2.13	8.07	7.08	0.38	10.61	14.35	–
Cr_2O_3	0.03	0.55	45.66	–	–	–	0.02	0.01	0.03	28.66	14.23	0.19	–	–	–
V_2O_5	–	–	0.25	–	–	–	–	–	–	0.31	0.5	0.52	–	–	–
FeO	10.49	4.09	23.18	4.72	0.29	1.30	14.25	16.26	4.55	42.94	57.14	35.18	6.78	6.99	0.51
MnO	0.16	0.04	0.23	0.02	0.00	0.00	0.19	0.22	0.08	0.33	0.35	0.35	0.06	0.04	0.02
MgO	48.08	15.69	12.87	22.24	6.44	0.55	45.44	43.87	15.95	9.64	8.16	10.77	16.98	20.91	1.61
NiO	0.36	–	0.19	–	–	–	0.18	0.15	–	0.2	0.17	0.09	–	–	–
CaO	0.06	23.22	0.00	0.06	49.13	0.05	0.15	0.17	22.29	0.01	0.02	0.1	11.13	0.07	52.47
Na_2O	–	0.53	–	0.34	0.02	14.95	0.15	0.17	0.93	0.01	0.02	0.1	3.11	1.18	0.04
SrO	–	–	–	–	0.06	–	–	–	–	0.11	0.22	0.13	–	–	0.02
K_2O	–	–	–	10.01	0.01	8.11	–	–	–	–	–	–	1.4	8.5	0.01
F	–	–	–	3.93	–	0.02	–	–	–	–	–	–	0.14	0.29	–
Cl	–	–	–	0.01	–	0.01	–	–	–	–	–	–	0.01	0.02	–
Total	99.12	98.88	99.59	98.13	55.98	99.58	99.63	99.95	99.19	97.98	97.39	99.60	96.71	94.47	55.70
Mg/(Mg + Fe)	0.89	0.87	0.50	0.89	0.98	0.43	0.85	0.83	0.86	0.29	0.20	0.35	0.82	0.84	0.85
Ca/(Ca + Mg + Fe)	–	–	–	–	0.84	–	–	–	–	–	–	–	–	–	0.95

Table 2 (Contd.)

	Labait 19 (LB19)				Pello Hill 2 (PEL2)									
	OL	CHRMT	PHLOG	CC	OL	OL Near vein	OPX Near vein	OPX Near vein	CPX In vein	RT In vein	CHRMT	AMPH In vein	PHLOG In vein	CC
SiO_2	39.98	0.06	39.06	0.02	40.39	40.54	56.43	56.63	53.82	0.03	0.06	45.82	38.95	0.10
TiO_2	0.04	5.26	3.63	–	0.00	0.02	0.04	0.13	0.61	96.35	0.15	3.25	0.80	–
Al_2O_3	0.02	7.48	13.63	–	0.03	0.01	1.95	1.35	2.15	0.15	21.62	9.39	16.02	–
Cr_2O_3	0.04	48.10	–	–	0.02	0.01	0.66	0.49	0.17	0.23	47.63	–	–	–
V_2O_5	–	0.34	–	–	–	–	–	–	–	0.97	0.25	–	–	–
FeO	12.33	22.50	4.74	0.15	6.70	7.86	4.21	4.99	2.55	0.61	13.57	3.18	2.63	0.09
MnO	0.16	0.24	0.04	0.01	0.11	0.10	0.08	0.11	0.08	0.00	0.19	0.05	0.04	0.02
MgO	47.30	12.31	22.11	2.58	50.45	49.80	35.41	34.92	17.80	0.04	16.47	19.65	23.78	2.82
NiO	0.33	0.19	0.02	–	0.38	0.35	–	–	–	0.00	0.16	–	–	–
CaO	0.07	0.01	–	52.45	0.05	0.07	0.52	0.72	20.83	0.02	0.01	10.29	0.03	50.88
Na_2O	–	–	0.62	0.00	–	–	0.10	0.12	1.11	–	–	3.60	1.64	0.03
SrO	–	–	–	0.03	–	–	–	–	–	–	–	–	–	0.18
K_2O	–	–	9.59	–	–	–	–	–	–	–	–	0.89	7.82	0.02
F	–	–	0.59	–	–	–	–	–	–	–	–	0.34	0.36	–
Cl	–	–	0.02	–	–	–	–	–	–	–	–	0.01	0.02	–
Total	100.27	96.49	94.05	55.24	98.13	98.76	99.40	99.46	99.12	98.40	100.11	96.47	92.09	54.14
Mg/(Mg + Fe)	0.87	0.49	0.89	0.97	0.93	0.92	0.94	0.93	0.93	0.10	0.68	0.92	0.94	0.98
Ca/(Ca + Mg + Fe)	–	–	–	0.93	–	–	–	–	–	–	–	–	–	0.93

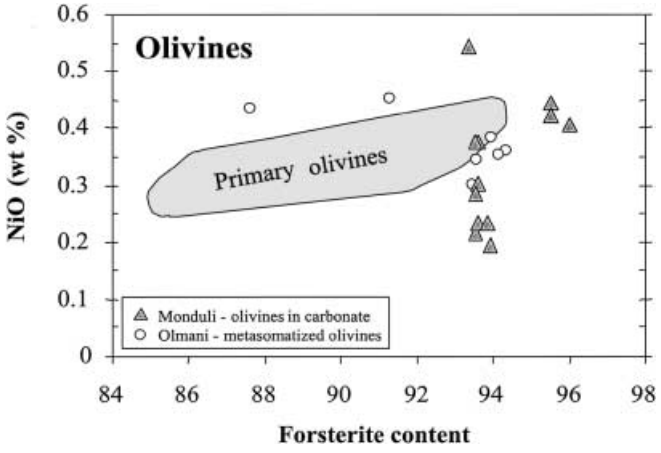

Fig. 2 NiO versus forsterite content in olivines. *Shaded field* represent primary olivines from Tanzanian xenoliths (Rudnick et al. 1993; C.-T. Lee and Rudnick 1999). *Circles* represent olivines from highly magnesian dunites and wehrlites at nearby Olmani volcano; these xenoliths are believed to have seen the reactive passage of carbonatitic melts (Rudnick et al. 1993)

The conservative approach taken here is to assume that these carbonates are of hydrothermal or surficial origin.

Bulk-rock geochemistry

Whole-rock major and trace element analyses were determined for four xenoliths: LB58, LB19, MON5, and MON7. The results are presented in Table 3 (analytical methods described in Appendix). Monduli xenoliths, MON5 and MON7, have very low incompatible trace element contents, as exemplified by the fact that some of the heavy rare-earth elements are slightly below the limit of detection (3σ + background). MON7 has trace element characteristics typical of carbonatite-metasomatized peridotites, namely high Ca/Al and depletion in some high field strength elements (HFSE) relative to rare-earth elements (REEs; e.g., low Zr/Sm and low Ti/Gd; Dupuy et al. 1992; Rudnick et al. 1993; Klemme et al. 1995). In contrast, Labait xenoliths LB58 and LB19 have higher incompatible trace element contents and their compositions are more typical of other peridotite xenoliths from Labait (C.-T. Lee and Rudnick, unpublished data): enrichment in light rare-earth elements (LREE) and high field strength elements over the heavy rare-earth elements (HREE). The metasomatic features of these xenoliths are believed to be derived from silicate-metasomatism because of the presence of metasomatic minerals, such as clinopyroxene, phlogopite, and rutile. In LB58 and LB19, clinopyroxene and phlogopite are volumetrically more significant than the carbonates.

Carbonate geochemistry

Nearly all carbonates are calcitic, ranging from Ca/(Ca + Mg + Fe) of 0.93 to pure calcite. The only exceptions are carbonates in LB58, which have a Ca/

Table 3 Whole-rock major element and trace element concentrations by ICP-MS and XRF. * indicates XRF analyses; all other elements determined by ICP-MS. < indicates below limit of detection so concentrations given should be taken as upper limit of possible values; *n* number of analyses; *SD* 1 standard deviation

	LB 19R	LB58			MON5			MON7		
	wt%	wt%	*n*	SD	wt%	*n*	SD	wt%	*n*	SD
SiO_2*	42.23	39.71	–	–	–	–	–	43.28	–	–
TiO_2*	0.09	0.10	–	–	–	–	–	0.00	–	–
Al_2O_3*	0.82	0.52	–	–	–	–	–	0.52	–	–
FeO tot*	8.51	10.50	–	–	–	–	–	6.08	–	–
MnO*	0.15	0.18	–	–	–	–	–	0.12	–	–
MgO*	45.76	45.05	–	–	–	–	–	47.69	–	–
CaO*	0.46	0.83	–	–	–	–	–	0.67	–	–
Na_2O*	0.00	0.00	–	–	–	–	–	0.00	–	–
K_2O*	0.25	0.09	–	–	–	–	–	0.01	–	–
P_2O_5*	0.01	0.01	–	–	–	–	–	0.00	–	–
Total	98.26	98.17	–	–	–	–	–	99.05	–	–
	ppm	ppm	–	–	–	–	–	ppm	–	–
Li	2.1	1.9	3	0.8	0.6	3	0.3	0.53	3	0.07
Sc	3.2	3.8	3	0.6	3	3	2	3	3	2
Ti*	525	670	2	68	–	–	–	27	1	–
V*	27	30	1	–	–	–	–	14	1	–
Cr*	2012	4345	1	–	–	–	–	2120	1	–
Ni*	2562	2834	1	–	–	–	–	2573	1	–
Zn*	56	71	1	–	–	–	–	41	1	–
Ga	0.65	0.58	3	0.09	–	–	–	0.21	3	0.04
Rb	6.2	6.3	3	0.6	0.44	3	0.06	0.43	3	0.08
Rb*	7.1	6.5	–	–	–	–	–	0.50	–	–
Sr	25	13	3	2	11	3	2	11	3	2
Sr*	30	13	–	–	–	–	–	12	–	–
Y	0.38	0.57	3	0.04	0.16	3	0.01	0.17	3	0.01
Y*	0.40	0.55	–	–	–	–	–	0.3	–	–
Zr	3.4	9.8	3	0.5	0.65	3	0.03	0.8	3	0.1
Zr*	4.0	10.1	–	–	–	–	–	1	–	–
Nb	1.2	2.1	3	0.0	0.46	3	0.01	0.58	3	0.02
Nb*	1.2	2.1	–	–	–	–	–	0.6	–	–
Cs	0.03	0.14	3	0.01	0.006	3	0.002	0.005	3	0.001
Ba	–	–	–	–	25	3	1	24	3	4
Ba*	1050	81	1	–	–	–	–	30	1	–
La	0.46	0.92	3	0.03	0.22	3	0.01	0.23	3	0.02
Ce	1.01	1.78	3	0.04	0.262	3	0.009	0.36	3	0.02
Pr	0.130	0.224	3	0.009	0.038	3	0.001	0.039	3	0.003
Nd	0.526	0.91	3	0.02	0.162	3	0.007	0.15	3	0.01
Sm	0.110	0.193	3	0.009	< 0.038	3	0.001	< 0.032	3	0.007
Gd	0.100	0.172	3	0.004	0.038	3	0.001	0.034	3	0.003
Tb	0.0147	0.0241	3	0.0003	< 0.005	3	0.001	< 0.005	3	0.001
Dy	0.076	0.126	3	0.004	0.029	3	0.005	0.029	3	0.005
Ho	0.014	0.023	3	0.001	< 0.005	3	0.001	< 0.006	3	0.001
Er	0.039	0.059	3	0.003	0.015	3	0.004	0.017	3	0.004
Yb	0.041	0.046	3	0.002	< 0.013	3	0.006	< 0.014	3	0.004
Lu	0.007	0.007	3	0.001	< 0.002	3	0.001	< 0.002	3	0.001
Hf	0.095	0.276	3	0.006	< 0.009	3	0.003	< 0.014	3	0.003
Th	0.042	0.083	3	0.002	0.06	3	0.02	0.05	3	0.01
U	0.009	0.025	3	0.001	0.07	3	0.02	0.05	3	0.01
Mg/(Mg + Fe)	90.6	88.4	–	–	–	–	–	93.3	–	–
Ca/Al	0.76	2.15	–	–	–	–	–	1.74	–	–
Ti/Gd	5226	3896	–	–	–	–	–	794	–	–

(Ca + Mg + Fe) ratio of 0.83 and ~6 wt% MgO. Mg/(Mg + Fe) ratios for all but one of these carbonates are greater than 0.9 [carbonates included in an olivine phenocryst in the lava rind of MON5 have Mg/(Mg + Fe) ratios of 0.6]. SiO_2 contents are mostly below 0.20 wt%. All carbonates are devoid of appreciable alkalis. A comparison of the Tanzanian mineral carbonate compositions to a global compilation electron microprobe analyses of carbonates from mantle-derived rocks is shown in the $CaCO_3$–$MgCO_3$ binary (Fig. 3). As can be seen, many of the carbonates reported in the literature are calcitic.

In situ trace element analyses of carbonates are given in Table 4. Most carbonates are characterized by high U (Th/U < 1) and Sr, but low total REE and HFSE contents, as exemplified by ΣREEs < 25 ppm (Fig. 4; Table 4). The low trace element abundances are similar to those measured for carbonates in spinel peridotite xenoliths from Spitsbergen and Mongolia (Ionov 1998).

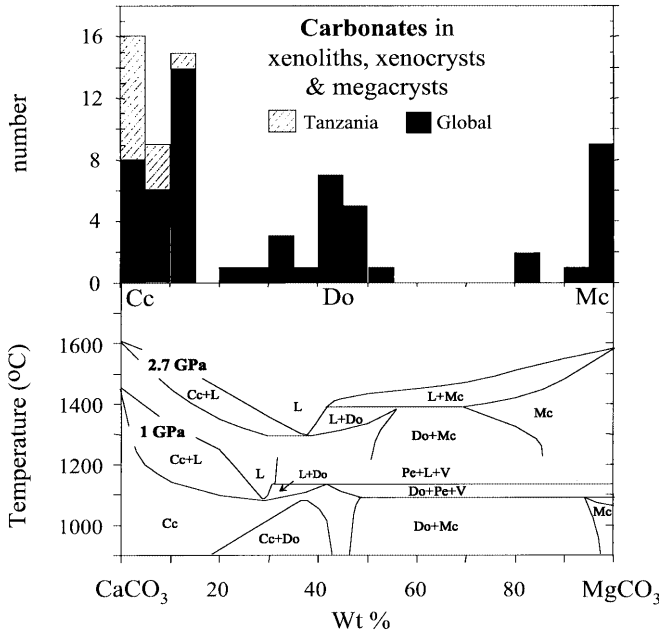

Fig. 3 Histogram of carbonate inclusion compositions in mantle-derived rocks (xenoliths, megacrysts, and xenocrysts). Phase diagram modified from Wyllie and W.-J. Lee (1998). The data are compiled from McGetchin and Besancon (1973), Hunter and Smith (1981), Berg (1986), Amundsen (1987), Smith (1987), Bulanova and Pavlova (1987), Ionov et al. (1993), Yang et al. (1993), Frezzotti et al. (1994), McInnes and Cameron (1994), Pyle and Haggerty (1994), Schiano et al. (1994), Zhang and Liou (1994), Kogarko et al. (1995), Ionov et al. (1996), and Ionov (1998). *Cc* Calcite, *Mc* magnesite, *Do* dolomite, *L* liquid, *Pe* periclase, *V* vapor

The latter manuscript also reported in high Sr and U in some carbonates. There is no clear distinction between hydrothermal carbonates and primary carbonates, but hydrothermal carbonates seem to have lower ΣREEs.

Stable isotope geochemistry of carbonates

Carbon and oxygen isotopic abundances were determined on selected carbonate patches (extracted using a micro-drill), two carbonatites (Oldoinyo Lengai and Labait), a lava rind (LB58r), a sovite xenolith (Kisite crater), and a caliche vein within a peridotite. Results are tabulated in Table 5 and shown in Fig. 5. The Oldoinyo Lengai carbonatite was collected probably within weeks of eruption (sample was collected black, but it turned to a gray color within several weeks after collecting it in July 1996) and analyzed within a year. The lava rind, sovite, and Oldoinyo Lengai carbonatite all plot near the primary carbonatite field, which broadly coincides with mantle $\delta^{13}C$ and $\delta^{18}O$. The carbonate inclusion in LB58 and the caliche (LB50) have heavy oxygen signatures, but have carbon signatures only slightly higher than the mantle range. This is the trend expected for low temperature meteoric exchange (Deines 1989; Horstmann and Verwoerd 1997). The high $\delta^{18}O$ values lie within the range for weathered natrocarbonatites and calcrete from Tanzania (Hay 1989).

The Labait carbonatite and the carbonate inclusions in MON7 also yield heavy oxygen signatures, but interestingly, have light carbon signatures. These light values are lower than any observed for carbonatites and calcite veins in peridotites (Deines 1968). They are similar, however, to eclogitic diamonds (Kirkley et al. 1991), CO_2-rich fluid inclusions in clinopyroxenes from peridotite xenoliths (Porcelli et al. 1992), and CO_2 in basalt glasses from mid-ocean ridges (DesMarais and Moore 1984). The origin of these light carbon signatures is highly debated, with models ranging from an origin by recycling of biogenic material to high temperature fractionation during devolatilization (Javoy et al. 1986; Mattey et al. 1990; Galimov 1991; Kirkley et al. 1991; Cartigny et al. 1998). The small amount of data in hand are not sufficient to distinguish between these different possibilities, so we are forced, for now, to treat these observations as curiosities.

Discussion

Primary origin of Tanzanian carbonates

The first matter of concern is to test whether the Tanzanian carbonates are primary, in the sense that they are not products of post-emplacement processes, such as hydrothermal and supergene alteration. The following characteristics are indicative of a primary origin (e.g., Ionov 1998): (1) association of carbonates with secondary refractory minerals (forsteritic olivine and spinel in Monduli carbonates), many of which are completely enclosed within the carbonate and have compositions differing from minerals associated with the primary peridotite assemblage and the host lava; (2) association of carbonates with magmatic minerals, such as nepheline (LB58); and (3) fully included carbonates within primary olivines with few or no cracks leading to the exterior of the host-olivine (MON5p and EL14). Based on these criteria, we interpret the carbonates in LB58, EL14, and in all Monduli xenoliths as precipitates formed before or during entrainment of the xenolith in the host magma.

In contrast, zeolites intergrown with carbonates in PEL2 and EL10 argue for carbonate-precipitation at low temperature, probably from hydrothermal solutions. Finally, we cannot assess the nature of the carbonates in LB19 because they lack diagnostic features (i.e., no secondary mineral inclusions, no reaction textures). In the following discussion, we thus consider only carbonates that are likely to be of mantle origin (Monduli samples, EL14, LB58).

Quenched liquids or crystalline solids?

Insights from the clinopyroxene-free Monduli harzburgites

Distinguishing quenched liquid from crystalline carbonate on the basis of texture is difficult. This matter has

Table 4 Trace element concentrations (in ppm) of carbonates determined by LA-ICP-MS. Individual spot analyses for all samples range from 50 to 100 μm. < indicates below detection limit so given concentrations should be taken as upper limit

	Primary				Hydrothermal alteration								
	LB58 Neph-bearing		EL14 Inclusion in Ol		PEL2 Zeolite-bearing patch			EL10 Zeolite-bearing vein			LB19 Intergranular		
Zn	2.61	11.38	< 1.02	1.65	< 2.08	2.51	2.99	1.09	1.45	30.43	2.51	3.62	4.28
Sr	719	631	116	320	1802	1482	670	636	834	826	1179	15	16
Y	3.00	0.78	< 0.03	0.16	< 0.05	< 0.03	0.04	0.49	0.04	0.53	< 0.02	0.16	0.20
Zr	0.64	29	0.25	0.27	< 0.13	< 0.15	0.15	0.26	< 0.09	5.20	< 0.08	0.2	0.67
Nb	0.33	0.99	0.28	0.14	< 0.13	0.23	0.28	0.44	0.08	4.16	0.10	0.13	0.36
La	5.82	0.65	0.06	0.19	< 0.04	0.03	0.15	1.39	< 0.03	1.07	< 0.02	0.43	0.17
Ce	7.76	0.89	< 0.01	0.21	< 0.03	0.04	0.32	0.15	< 0.01	2.69	< 0.01	0.09	0.11
Nd	3.27	0.59	0.05	0.12	< 0.15	< 0.12	< 0.11	1.19	< 0.07	1.16	< 0.07	0.35	0.12
Sm	0.58	< 0.19	< 0.07	< 0.12	< 0.22	< 0.17	< 0.16	0.19	< 0.09	< 0.28	< 0.11	< 0.19	< 0.07
Eu	0.16	0.04	< 0.02	< 0.03	< 0.04	< 0.04	< 0.04	0.05	< 0.02	< 0.06	< 0.02	< 0.04	< 0.01
Gd	0.55	0.14	< 0.07	< 0.15	< 0.15	< 0.11	< 0.17	0.12	< 0.09	< 0.33	< 0.11	< 0.17	< 0.06
Dy	0.40	0.17	< 0.03	< 0.04	< 0.08	< 0.05	< 0.05	0.08	< 0.03	0.12	< 0.03	< 0.05	0.02
Ho	0.09	0.03	< 0.01	< 0.01	< 0.02	< 0.01	< 0.02	0.01	< 0.01	< 0.03	< 0.01	< 0.02	< 0.01
Er	0.23	0.09	< 0.02	< 0.02	< 0.04	< 0.04	< 0.03	0.03	< 0.01	< 0.08	< 0.02	< 0.05	< 0.02
Yb	0.27	0.12	< 0.01	< 0.03	< 0.05	< 0.03	< 0.03	0.03	0.02	< 0.07	< 0.02	< 0.03	< 0.02
Lu	0.03	0.02	< 0.01	< 0.02	< 0.02	< 0.02	< 0.02	< 0.01	< 0.01	< 0.02	< 0.01	< 0.02	< 0.01
Hf	< 0.02	0.77	< 0.02	< 0.04	< 0.05	< 0.04	< 0.05	< 0.01	< 0.02	0.10	< 0.02	< 0.06	0.02
Ta	< 0.30	0.08	< 0.01	< 0.01	< 0.01	0.01	0.02	< 0.01	< 0.01	0.14	< 0.01	< 0.02	0.01
Pb	0.30	0.51	0.04	< 0.23	< 0.09	0.14	0.08	0.11	0.03	2.02	< 0.08	0.64	0.28
Th	0.10	0.05	< 0.01	< 0.01	< 0.01	< 0.08	< 0.01	n.d.	n.d.	0.17	< 0.01	< 0.01	n.d.
U	0.23	0.23	< 0.03	0.14	0.08	0.12	0.08	0.14	0.07	0.22	0.12	0.06	0.06
ΣREE	19.16	< 2.93	< 0.36	< 0.94	< 0.84	< 0.66	< 1.10	3.24	< 0.39	< 5.91	< 0.43	< 0.57	< 0.20

	Primary										
	MON5					MON7				MON3 Xenocryst in lava		
	Inclusions in Ol phenocryst				Intrgrnlr	Intrgrnlr (1)		Intrgrnlr (2)				
Rb	< 0.13	< 0.11	< 0.14	< 0.11	2.83	< 0.31	< 0.40	< 0.25	< 1.58	< 0.07	< 0.12	< 0.13
Sr	248	234	190	770	515	222	250	391	365	132	129	186
Y	1.40	0.67	1.20	0.54	0.08	0.45	0.23	2.63	1.09	0.40	0.49	1.19
Zr	< 0.07	< 0.07	< 0.09	0.63	2.79	2.67	1.84	5.06	3.01	0.28	0.29	1.12
Nb	0.06	0.06	0.51	0.71	15	5.69	7.28	9.3	5.62	0.57	0.5	1.28
Cs	< 0.03	< 0.03	< 0.04	< 0.04	< 0.10	< 0.09	< 0.10	< 0.07	< 0.56	< 0.03	< 0.04	< 0.04
Ba	6.71	3.63	7.64	0.49	127	0.19	1.47	7.31	0.48	0.30	0.28	0.71
La	11.7	5.57	3.15	1.55	0.28	0.99	0.40	4.86	1.74	0.69	0.92	1.02
Ce	10.4	3.58	1.98	1.06	0.38	3.87	1.57	4.8	2.05	0.53	0.74	1.08
Nd	1.73	0.48	0.37	0.20	0.16	0.44	< 0.21	1.69	< 0.70	0.12	0.20	0.30
Sm	0.14	< 0.06	0.07	< 0.06	< 0.12	< 0.20	< 0.24	0.24	< 1.19	< 0.05	< 0.04	< 0.04
Eu	0.03	< 0.02	< 0.02	< 0.01	< 0.04	< 0.05	< 0.07	< 0.05	< 0.35	< 0.01	< 0.01	< 0.02
Gd	0.16	< 0.05	0.08	< 0.03	< 0.16	0.14	< 0.19	0.20	< 1.03	< 0.04	< 0.05	< 0.07
Dy	0.16	0.05	0.09	< 0.03	< 0.05	< 0.09	< 0.10	0.20	< 0.50	0.06	< 0.03	0.06
Ho	0.05	0.01	0.04	0.01	< 0.01	< 0.02	< 0.03	0.04	< 0.13	< 0.01	0.02	0.02
Er	0.10	0.04	0.10	0.02	< 0.05	< 0.08	< 0.06	0.24	< 0.28	0.02	0.05	0.11
Tm	0.03	0.01	0.02	< 0.01	< 0.01	< 0.02	< 0.03	0.02	< 0.09	< 0.01	< 0.01	0.02
Yb	0.15	0.05	0.10	0.05	< 0.04	< 0.05	< 0.10	0.21	< 0.21	0.02	0.04	0.10
Lu	0.01	0.01	0.01	0.01	< 0.02	< 0.02	< 0.02	0.03	< 0.11	< 0.01	0.01	0.01
Hf	< 0.02	< 0.03	< 0.02	< 0.02	0.05	< 0.07	< 0.12	< 0.04	< 0.37	< 0.02	< 0.02	< 0.03
Ta	< 0.01	n.d.	< 0.01	0.01	0.33	< 0.02	0.05	0.10	< 0.09	< 0.01	< 0.01	n.d.
Th	< 0.01	< 0.01	< 0.01	0.06	0.11	< 0.03	0.12	0.17	< 0.26	0.07	0.06	0.17
U	0.48	0.36	0.23	9.10	4.09	6.24	3.39	4.12	1.04	2.48	2.68	1.72
ΣREE	22.25	< 5.70	< 5.13	< 2.61	< 0.66	< 4.86	< 1.97	< 9.66	< 3.79	< 1.22	< 1.66	< 2.1

been thoroughly reviewed by W.-J. Lee et al. (1994) and is not discussed here. We simply note that all xenolith-hosted carbonate inclusions in this study have uniform extinction or have interlocking domains of uniform extinction. These textures do not resemble dendritic textures. Taken at face value, such carbonates do not look like quenched liquids.

We can gain further insight from the trace element content of the carbonates. As shown in Fig. 4, all the carbonates have ΣREE < 25 ppm. On the other hand,

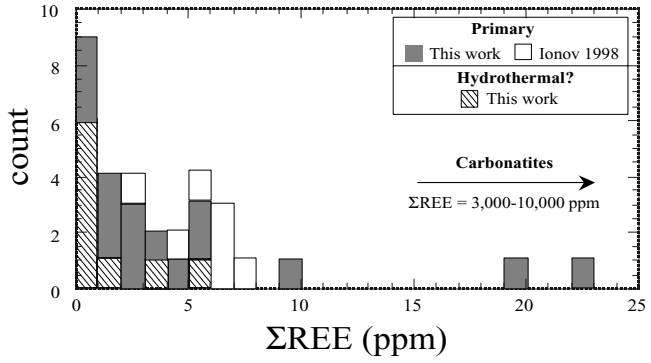

Fig. 4 Histogram of total rare-earth element contents in primary carbonates and in carbonates believed to have been derived from hydrothermal or supergene environments. Note that rare-earth element totals represent maximum values (see Table 4). Trace element composition of carbonatites taken from Woolley and Kempe (1989)

carbonatites have between 3000 and 10,000 ppm (based on calcio-, magnesio-, and natro-carbonatite compositions compiled by Woolley and Kempe 1989). The carbonate inclusions thus cannot represent quenched carbonatite lavas. However, the high Ca/Al and the low Ti/Gd of MON7 strongly suggest a carbonatitic component has been added to the whole-rock. Thus, one remaining question regards the residence of the rest of the incompatible trace elements if they are not accounted for by the carbonate phases. Because this phase escaped visual and back-scattered electron imaging detection, we conclude that its modal abundance is very low compared to the calcites themselves, and hence its REE content is very high.

While the foregoing suggests that the carbonates are not quenched melts, the trace element data, alone, leave us with two alternatives. One possibility is that the carbonates are quenched forms of an immiscible carbonate liquid. For example, a primary carbonate melt injected into the xenolith could differentiate to form conjugate silicate and carbonate liquids, and, because REEs are partitioned slightly more into the silicate melt (Wendlandt and Harrison 1979; Hamilton et al. 1989; Jones et al. 1995; Veksler et al. 1998), the conjugate carbonate melt could be lower in total REE abundance. Alternatively, the carbonates could represent crystal precipitates from a primary carbonated melt, leaving a trace element-enriched residual liquid.

Insights from other observations of mantle carbonates

Major element compositions of carbonate grains from mantle-derived rocks worldwide (xenoliths, xenocrysts, and megacrysts) are presented graphically in Fig. 3. The binary $CaCO_3$–$MgCO_3$ phase diagram in Fig. 3 is modified from Wyllie and W.-J. Lee (1998) and is used here to compare natural carbonate compositions to experimental compositions. Although the Ca–Mg binary simplifies the natural system, it approximates the natural carbonates compiled from the literature because most are devoid of Si, Na, and K.

The important point to note from Fig. 3 is that carbonate grains, including the calcites in this study, do not show a continuous compositional distribution. Instead, their compositions are clustered at nearly pure calcite, pure magnesite, and stoichiometric dolomite. Only a few carbonates have compositions overlapping the compositions expected for eutectic liquids (calcic dolomite). If carbonate inclusions worldwide are quenched liquids, then a peak at eutectic compositions would be expected. This compositional distribution suggests that the calcites in this study, as well as the majority of carbonate grains worldwide, are crystalline precipitates from carbonate melts. If so, determining the actual carbonate melt composition would require reconstruction of mineral grains. Dalton and Wood (1993a) and W.-J. Lee and Wyllie (1998) have also shown that neither primary carbonatitic melts nor immiscible carbonate liquids become significantly more calcitic than 80 wt% $CaCO_3$, due to the large carbonate liquidus volume, which generates a forbidden zone for magma compositions (W.-J. Lee and Wyllie 1998). Low trace element abundance may thus be an additional diagnostic feature of crystalline carbonate in mantle rocks.

Table 5 Stable isotope compositions of carbonate inclusions, carbonatites, caliche, and sovites

		$\delta^{18}O/^{16}O$ SMOW			$\delta^{13}C/^{12}C$ PDB		
			n	SD		*n*	SD
Monduli							
Mon 7	Peridotite	25	3	1.1	−16	3	1.0
Labait							
LB50	Caliche in peridotite	27	1		−2.9	1	
LB58	Peridotite	23	1		−2.5	1	
LB52	Carbonatite	26.0	4	0.71	−12.2	4	0.82
LB58r	Carbonate in basalt	11	2	1.6	−4.1	2	0.16
Carbonatites and sovites							
Ol Doinyo Lengai	Natrocarbonatite	11.8	1		−6.4	1	
KS6	Sovite	10	2	1.0	−4.18	2	0.07

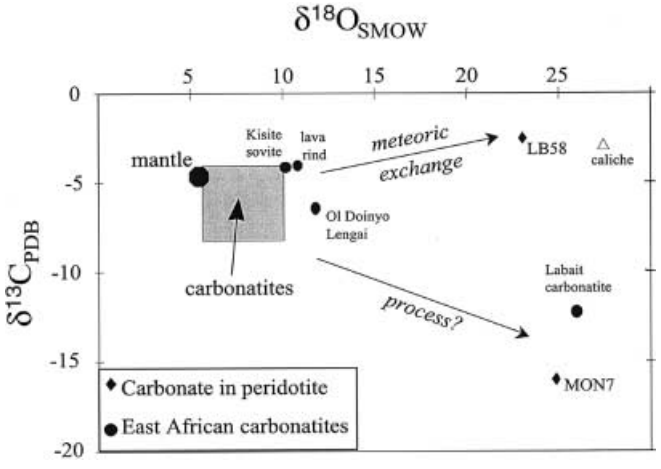

Fig. 5 Stable isotope data for carbonate inclusions and East African carbonatites and sovites. Carbon isotopic ratios are relative to PDB standard and oxygen ratios are relative to SMOW. Primary carbonatite field taken from Keller and Hoefs (1995). MON7 and LB58 represent primary calcite inclusions. Caliche is from a crosscutting vein in a peridotite (LB50). Oldoinyo Lengai represents a fresh carbonatite lava collected from the summit caldera and analyzed within the following year. Kisite sovite is a xenolith collected from the Kisite tuff cone, just south of Oldoinyo Lengai. "Lava rind" refers to a microdrilled portion of the rind to LB58 (LB58r), one of the carbonate-bearing peridotite xenoliths discussed in the text. Labait carbonatite represents an altered sample taken from the tuff cone

Speculations on petrogenetic origin

Decompressional crystallization of a primary carbonate melt

The occurrence of calcite in the Monduli harzburgites is probably a disequilibrium feature because pure calcite is not stable in mantle harzburgite. Since we see no evidence for the reaction dolomite + orthopyroxene = olivine + calcite + CO_2 or for any other reaction, introduction of carbonate must have occurred shortly before eruption.

One possible explanation for these observations is that the magnesian olivines precipitated directly out of a carbonate melt undergoing decompression. As shown in Fig. 6, the positions of the phase boundaries in the CO_2-saturated SiO_2–CaO–MgO pseudoternary system vary considerably with pressure. The vapor-saturated olivine liquidus field expands considerably from ~2.8 to ~1 GPa because the olivine–clinopyroxene cotectic curve occurs at lower MgO bulk compositions with decreasing pressure. In addition, with increasing pressure, the olivine–clinopyroxene cotectic gradually disappears as the melt–lherzolite equilibrium point (denoted by a star in Fig. 6) approaches the olivine–clinopyroxene–carbonate–melt equilibrium point. At ~2.8 GPa, the two points converge, forming an invariant eutectic point where lherzolite, carbonate, and melt are in equilibrium (this is point Q in Wyllie and W.-J. Lee 1998). At pressures greater than 2.8 GPa, the orthopyroxene liquidus field expands, resulting in the complete separation of the olivine and clinopyroxene liquidus fields. In Fig. 6, we show the permissible liquid compositions for which decompressional crystallization could lead to the initial precipitation of olivine followed by calcite (shaded fields), yielding the distinctive calcite patches with "floating" olivines. For example, between 2.7 and 2.8 GPa, a carbonatitic liquid could be in equilibrium with lherzolite. If rapidly decompressed, the liquid composition would lie in the olivine liquidus field, and would thus precipitate olivine upon cooling. Precipitation of olivine would drive the liquid composition toward the divariant calcite–olivine coprecipitation line

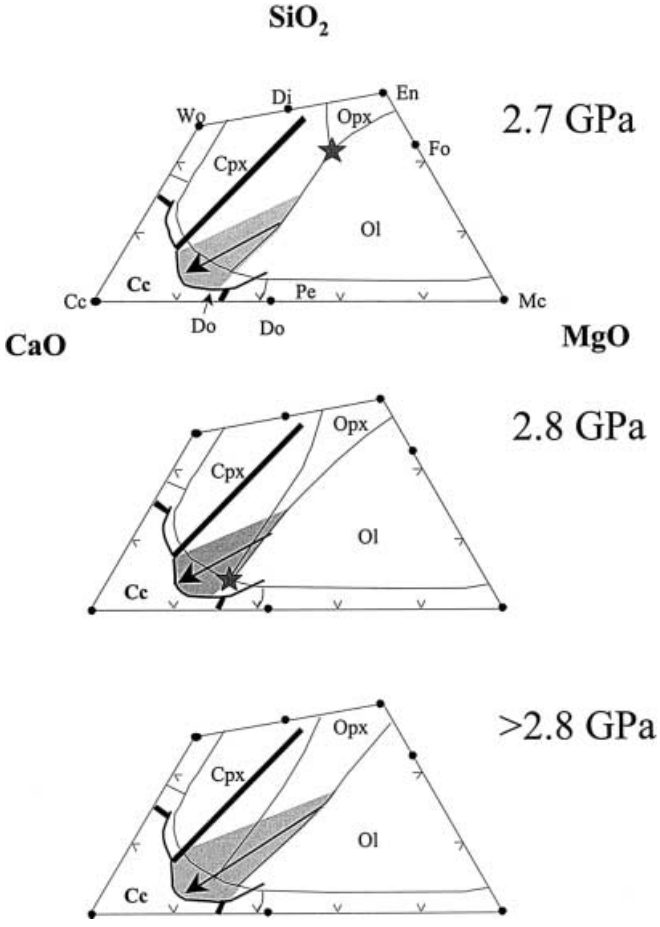

Fig. 6 CO_2-vapor-saturated liquidus fields in the CaO–MgO–SiO_2 (mole %) pseudoternary system (adapted from Wyllie and Huang 1976; Wyllie and W.-J. Lee 1998; and W.-J. Lee and Wyllie, 2000). *Thick lines* represent coprecipitation lines at ~1 GPa. *Thin lines* represent coprecipitation lines at 2.7, 2.8, and >2.8 GPa (top, middle, and lower panels, respectively). *"Star" symbol* represents the point at which carbonatitic melt is in equilibrium with lherzolite. At 2.8 GPa, this point coincides with the calcite liquidus surface, creating an invariant point at which lherzolite is in equilibrium with calcite and melt. *Shaded regions* show the permissible liquid compositions for which decompressional crystallization will lead to the precipitation of olivine and calcite. *Arrow* denotes the direction in which the liquid composition changes as olivine precipitates. *Cc* Calcite, *Do* dolomite, *Pe* periclase, *Mc* magnesite, *Fo* forsterite, *En* enstatite, *Di* diopside, *Wo* wollastonite, *Ol* olivine, *Opx* orthopyroxene, *Cpx* clinopyroxene

(forsterite + calcite + CO_2 vapor = liquid), thus precipitating calcite. At pressures greater than ~2.8 GPa, even liquids originally in equilibrium with harzburgite can give rise to olivine–calcite intergrowths if decompressed rapidly enough. W.-J. Lee and Wyllie (1998) have shown that these precipitated calcites are extremely low in Mg and Fe, similar to the observations presented here. Thus, the calcite–olivine intergrowths at Monduli may have formed as a primary carbonatitic liquid was injected into peridotitic wallrock at fairly high pressures (~2.8 GPa) just before eruption. This is followed immediately by eruption of the host lava and rapid entrainment of the wallrock as a xenolith, during which the xenolith decompressed so rapidly that the trapped carbonatitic liquid precipitated olivine and calcite before reacting with the host harzburgite.

For the formation of the calcite inclusions in olivine phenocrysts (MON5p) and primary dunitic olivines (EL14), we envision a slightly different scenario. While Dalton and Wood (1993b) showed that calcite is stable in a lherzolitic (i.e., clinopyroxene-bearing) mantle between 1.5 and 2.5 GPa and 750 and 1000 °C, the calcites in MON5p and EL14 are associated with olivine. One possibility for the coexistence of olivine and calcite in the absence of pyroxenes, however, is formation via the reaction forsterite + calcite + CO_2 vapor = liquid, as discussed in the preceding paragraph. If this interpretation is correct, then the calcites in EL14 and in MON5p are low pressure magmatic cumulates, as are their olivines. The bulk Fe-rich nature of EL14 may be indicative of a cumulate (or melt–wallrock reaction) origin. The calculated olivine–calcite Fe–Mg K_D's (X_{Fe}^{carb} XMg^{ol}/$XFe^{ol}XMg^{carb}$) for EL14 are ~1, which is close to equilibrium. On the other hand, for MON5p, one carbonate–olivine pair gives a K_D of ~0.4 while a second carbonate in the same olivine phenocryst gives a K_D of 4.

Low pressure injection by host lava

Calcites in LB58 were also introduced very recently, perhaps during eruption, because reaction textures are lacking, and Fe–Mg exchange K_D's are ~0.2 between calcite and primary olivines, indicating disequilibrium. The presence of nepheline suggests that the parent melt was an undersaturated silicate melt. Based on W.-J. Lee and Wyllie's (1996, 1998) phase diagrams in (MgO + FeO)–(Na_2O + K_2O)–(CaO)–(SiO_2 + Al_2O_3 + TiO_2) space, one possible liquid line of descent may be the initial precipitation of silicate minerals from a nephelinite or melilitite, followed by precipitation of calcite when the residual liquid intersects the carbonate liquidus.

Conclusions

The first occurrences of primary carbonate inclusions in mantle xenoliths from the East African Rift show the following features:

1. All carbonates are calcitic, with little or no Si, K, or Na.
2. The carbonates occur as intergranular patches and as inclusions in primary olivine grains.
3. The primary carbonates show little or no reaction with the host xenolith, but some contain euhedral mineral inclusions, such as olivine, spinel, and nepheline.
4. The carbonates exhibit uniform extinction or contain domains of uniform extinction.
5. Most carbonates have very low trace element contents and cannot account for the whole-rock trace element abundances of highly incompatible elements.

Based on these observations, we draw the following conclusions:

1. Those carbonates that are entirely included within olivine or those containing associated upper mantle phases (i.e., olivine and spinel) are probably crystalline precipitates from a carbonate melt within the mantle or during ascent in the host lava.
2. These carbonates have low trace element abundances, which may be an additional tool for distinguishing crystalline carbonate from quenched carbonate liquid.
3. Because carbonates in mantle-derived rocks worldwide are generally calcite, magnesite or dolomite rather than eutectic carbonate compositions (calcic dolomite), most are probably crystalline precipitates.
4. The Tanzanian calcites intergrown with zeolites are probably post-eruption hydrothermal precipitates.

Acknowledgments We thank J. Chesley and A. Tesha for assisting during fieldwork, the Tanzanian government and Dorobo Safaris for logistical help in the field, J. Bartley, B. Marino, and D. Schrag for oxygen and carbon isotope analyses, and D. Lange for help in electron microprobe analyses. D. Canil, J. Dalton, W.-J. Lee, R. Luth, A. Saal, and G. Yaxley provided much insight. W.-J. Lee and P. Wyllie are thanked for allowing the use of preprint material, and D. Ionov and the late Vera G. Steghey are thanked for insightful comments on the manuscript. This research was supported by NSF grant EAR 9506510 (R. L. Rudnick and J. T. Chesley), grant EAR-9711008 (R. L. Rudnick and W. F. McDonough), and an NSF graduate fellowship to C.-T. Lee.

Appendix: analytical methods

Mineral compositions

Electron microprobe analysis was done on the Harvard Cameca MBX microprobe using wavelength dispersive spectrometers (10–15 nA beam currents and 15 kV accelerating voltage). Matrix correction was done using the Sandia Bence-Albee 85 program.

Bulk-rock geochemistry

Samples for bulk trace element analysis were dissolved in a mixture of Seastar HF–HNO_3 in Savillex Teflon beakers and then dried down. The residue was taken up in 2% HNO_3 and then spiked with a mixed multi-element/enriched isotope internal standard solution prior to analysis (Eggins et al. 1997). Bulk-rock trace elements were determined by inductively coupled plasma-mass spectrometry

(ICP-MS) using a PQ II+ (VG Elemental) in pulse counting mode (three points per peak). Dwell time and quadrupole settling times were 10 and 5 ms, respectively. Transition elements (Ti, V, Cr, Ni, Zn) and major elements were determined by conventional X-ray fluorescence techniques at the University of Massachusetts, Amherst.

In situ trace element geochemistry

In situ trace element analysis of the carbonates was done using laser ablation ICP-MS. A Lambda Physik excimer laser (Compex 110, using an argon fluoride mixture to produce 193 nm laser light) was used. The design of the optics system is discussed in Horn et al. (2000). Spot sizes used in this study ranged from 50 to 100 μm. Trace elements were analyzed on a PQ II+ (VG Elemental) ICP-MS. Analyses were performed in peak hopping mode using one point per peak with a dwell time of 6 ms and a quadrupole settling time of 6 ms. Total acquisition time for an analysis varied between 120 and 300 s, depending on the spot size and thickness of the carbonates. Laser ablation sensitivity of up to 7000 cps/ppm for a 40 μm spot (pulse energy ~0.3 mJ) was obtained with the aid of flushing the sample cell with He (Eggins et al. 1998; Horn et al. 2000). The acquisition and calculation of transient signals follow methods described in Longerich et al. (1996), using ^{43}Ca as the internal standard (determined by EMPA).

Stable isotope geochemistry

Carbon and oxygen isotopic compositions were determined at Harvard using a VG Isogas Prism mass spectrometer with triple collectors. Carbonates were extracted directly from the rock by microdrilling. The drilled powders were reacted with H_3PO_4 in sealed tubes at 90 °C, and the resulting carbon dioxide was distilled on a vacuum line. For a few analyses, reaction with phosphoric acid was done on-line. Details of the analytical precision, accuracy, and fractionation corrections are discussed in Kaufman and Knoll (1995) and Bartley et al. (1998).

References

Amundsen HEF (1987) Evidence for liquid immiscibility in the upper mantle. Nature 327: 692–695

Barker DS (1996) Consequences of recycled carbon in carbonatites. Can Mineral 34: 373–387

Bartley JK, Pope M, Knoll AH, Semikhatov MA, Petrov PY (1998) A Vendian–Cambrian boundary succession from the northwestern margin of the Siberian Platform: stratigraphy, palaeontology, chemostratigraphy and correlation. Geol Mag 135: 473–494

Berg GW (1986) Evidence for carbonate in the mantle. Nature 324: 50–51

Bulanova GP, Pavlova LP (1987) Magnesite– peridotite mineral association in a diamond. Dokl Akad Nauk SSSR 295: 1452–1456

Canil D (1990) Experimental study bearing on the absence of carbonate in mantle-derived xenoliths. Geology 18: 1011–1013

Cartigny P, Harris JW, Javoy M (1998) Eclogitic diamond formation at Jwaneng: no room for a recycled component. Science 280: 1421–1424

Chesley JT, Rudnick RL, Lee C-T (1999) Re–Os systematics of mantle xenoliths from the East African rift: age, structure, and history of the Tanzanian craton. Geochim Cosmochim Acta 63: 1203–1217

Coltorti M, Bonadiman C, Hinton RW, Siena F, Upton BGJ (1999) Carbonatite metasomatism of the oceanic upper mantle: evidence from clinopyroxenes and glasses in ultramafic xenoliths of Grande Comore, Indian Ocean. J Petrol 40: 133–165

Dalton JA, Wood BJ (1993a) The compositions of primary carbonate melts and their evolution through wallrock reaction in the mantle. Earth Planet Sci Lett 119: 511–525

Dalton JA, Wood BJ (1993b) The partitioning of Fe and Mg between olivine and carbonate and the stability of carbonate under mantle conditions. Contrib Mineral Petrol 114: 501–509

Dautria JM, Dupuy C, Takherist D, Dostal J (1992) Carbonate metasomatism in the lithospheric mantle: peridotitic xenoliths from a melilititic district of the Sahara basin. Contrib Mineral Petrol 111: 37–52

Dawson JB (1992) Neogene tectonics and volcanicity in the North Tanzania sector of the Gregory Rift Valley: contrasts with the Kenya sector. Tectonophysics 204: 81–92

Dawson JB (1999) Metasomatism and melting in spinel peridotite xenoliths from Labait, Tanzania. In: Gurney JJ, Gurney JL, Pascoe MD, Richardson SH (eds), The Dawson volume, Proc 7th Int Kimberlite Conf, Cape Town, pp 164–173

Dawson JB, Smith JV (1988) Metasomatized and veined upper-mantle xenoliths from Pello Hill, Tanzania: evidence for anomalously-light mantle beneath the Tanzanian sector of the East African Rift Valley. Contrib Mineral Petrol 100: 510–527

Dawson JB, James D, Paslick C, Halliday AM (1997) Ultrabasic potassic low-volume magmatism and continental rifting in north–central Tanzania: association with enhanced heat flow. Proc 6th Int Kimberlite Conf, Russ Geol Geophys 38: 69–81

Deines P (1968) The carbon and oxygen isotopic composition of carbonates from a mica peridotite dike near Dixonville, Pennsylvania. Geochim Cosmochim Acta 32: 613–625

Deines P (1989) Stable isotope variations in carbonatites. In: Bell K (ed) Carbonatites: genesis and evolution. Unwin Hyman, London, pp 301–359

DesMarais DJ, Moore JG (1984) Carbon and its isotopes in mid-oceanic basaltic glasses. Earth Planet Sci Lett 69: 43–57

Dobson DP, Jones AP, Rabe R, Sekine T, Kurita K, Taniguchi T, Kondo T, Kato T, Shimomura O, Urakawa S (1996) In-situ measurement of viscosity and density of carbonate melts at high pressure. Earth Planet Sci Lett 143: 207–215

Dupuy C, Liotard JM, Dostal J (1992) Zr/Hf fractionation in intraplate basaltic rocks: carbonate metasomatism in the mantle source. Geochim Cosmochim Acta 56: 2417–2423

Ebinger C, Djomani P, Mbede E, Foster A, Dawson JB (1997) Rifting Archaean lithosphere: the Eyasi–Manyar–Natron rifts, East Africa. J Geol Soc Lond 154: 947–960

Eggins SM, Woodhead JD, Kinsley L, Mortimer GE, Sylvester P, McCulloch MT, Hergt JM, Handler MR (1997) A simple method for the precise determination of >40 trace elements in geological samples by ICP-MS using enriched isotope internal standardisation. Chem Geol 134: 311–326

Eggins SM, Kinsley LPJ, Shelley JMG (1998) Deposition and element fractionation processes during atmospheric pressure laser sampling for analysis by ICP-MS. App Surf Sci 127–129: 278–286

Evans AL, Fairhead JD, Mitchell JG (1971) Potassium–argon ages from the volcanic province of northern Tanzania. Nature 229: 19–20

Frezzotti M-L, Touret JLR, Lustenhouwer WJ, Neumann E-R (1994) Melt and fluid inclusions in dunite xenoliths from La Gomera, Canary Islands: tracking the mantle metasomatic fluids. Eur J Mineral 6: 805–817

Galimov EM (1991) Isotope fractionation related to kimberlite magmatism and diamond formation. Geochim Cosmochim Acta 55: 1697–1708

Green DH, Wallace ME (1988) Mantle metasomatism by ephemeral carbonatite melts. Nature 336: 459–462

Hamilton DL, Bedson P, Esson J (1989) The behaviour of trace elements in the evolution of carbonatites. In: Bell K (ed) Carbonatites, genesis and evolution. Unwin Hyman, London, pp 405–427

Hauri EH, Shimizu N, Dieu JJ, Hart SR (1993) Evidence for hotspot-related carbonatite metasomatism in the oceanic upper mantle. Nature 365: 221–227

Hay RL (1989) Holocene carbonatite–nephelinite tephra deposits of Ol Doinyo Lengai, Tanzania. J Volcan Geotherm Res 37: 77–91

Horn I, Rudnick RL, McDonough WF (2000) Precise elemental and isotope ratio determination by simultaneous solution nebulization and laser ablation-ICP-MS: application to U–Pb geochronology. Chem Geol 164: 281–301

Horstmann UE, Verwoerd WJ (1997) Carbon and oxygen isotope variations in southern African carbonatites. J Afr Earth Sci 25: 115–136

Hunter WC, Smith D (1981) Garnet peridotite from Colorado Plateau ultramafic diatremes: hydrates, carbonates, and comparative geothermometry. Contrib Mineral Petrol 76: 312–320

Ionov D (1998) Trace element composition of mantle-derived carbonates and coexisting phases in peridotite xenoliths from alkali basalts. J Petrol 39: 1931–1941

Ionov DA, Dupuy C, O'Reilly SY, Kopylova MG, Genshaft YS (1993) Carbonated peridotite xenoliths from Spitsbergen: implications for trace element signature of mantle carbonate metasomatism. Earth Planet Sci Lett 119: 283–297

Ionov DA, O'Reilly SY, Genshaft YS, Kopylova MG (1996) Carbonate-bearing mantle peridotite xenoliths from Spitsbergen: phase relationships, mineral compositions and trace element residence. Contrib Mineral Petrol 125: 375–392

Javoy M, Pineau F, Delorme H (1986) Carbon and nitrogen isotopes in the mantle. Chem Geol 57: 41–62

Jones JH, Walker D, Picket DA, Murrel MT, Beate P (1995) Experimental investigations of the partitioning of Nb, Mo, Ba, Ce, Pb, Ra, Th, Pa, and U between immiscible carbonate and silicate liquids. Geochim Cosmochim Acta 59: 1307–1320

Kaufman AJ, Knoll AH (1995) Neoproterozoic variations in the C-isotopic composition of seawater: stratigraphic and biogeochemical implications. Precambrian Res 74: 27–49

Keller J, Hoefs J (1995) Stable isotope characteristics of recent natrocarbonatites from Oldoinyo Lengai. In: Bell K, Keller J (eds) Carbonatite volcanism, Oldoinyo Lengai and the petrogenesis of natrocarbonatites. Springer, Berlin Heidelberg New York, pp 113–123

Keller J, Spettel B (1995) The trace element composition and petrogenesis of natrocarbonatites. In: Bell K, Keller J (eds) Carbonatite volcanism, Oldoinyo Lengai and the petrogenesis of natrocarbonatites. Springer, Berlin Heidelberg New York, pp 70–86

Kirkely MB, Gurney JJ, Otter ML, Hill SJ, Daniels LR (1991) The application of C isotope measurements to the identification of the sources of C in diamonds: a review. Applied Geochem 6: 477–494

Klemme S, van der Laan SR, Foley SF, Gunther D (1995) Experimentally determined trace and minor element partitioning between clinopyroxene and carbonatite melt under upper mantle conditions. Earth Planet Sci Lett 133: 439–448

Kogarko LN, Henderson CMB, Pacheco H (1995) Primary Ca-rich carbonatite magma and carbonate–silicate–sulphide liquid immiscibility in the upper mantle. Contrib Mineral Petrol 121: 267–274

Law KM, Blundy JD, Wood BJ, Ragnarsdottir KV (1999) An investigation of the crystal chemical controls on trace element partitioning between carbonated melts and wollastonite, witherite and calcite. EOS 80: 357

Lee C-T, Rudnick RL (1999) Compositionally stratified cratonic lithosphere: petrology and geochemistry of peridotite xenoliths from the Labait tuff cone, Tanzania. In: Gurney JJ, Gurney JL, Pascoe MD, Richardson SH (eds), The Nixon volume, Proc 7th Int Kimberlite Conf, pp 503–521

Lee W-J, Wyllie PJ (1996) Liquid immiscibility in the join $NaAlSi_3O_8$–$NaAlSiO_4$–$CaCO_3$ to 2.5 GPa and the origin of calciocarbonatite magmas. J Petrol 37: 1125–1152

Lee W-J, Wyllie PJ (1998) Petrogenesis of carbonatite magmas from mantle to crust, constrained by the system CaO–(MgO + FeO*)–(Na_2O + K_2O)–(SiO_2 + Al_2O_3 + TiO_2)–CO_2. J Petrol 39: 495–517

Lee W-J, Wyllie PJ (2000) The system CaO–MgO–SiO_2–CO_2 at 1 GPa, metasomatic wehrlites, and primary carbonatite magmas. Contrib Mineral Petrol 138: 214–228

Lee W-J, Wyllie PJ, Rossman GR (1994) CO_2-rich glass, round calcite crystals, and no liquid immiscibility in the system CaO–SiO_2–CO_2 at 2.5 GPa. Am Mineral 79: 1135–1144

Longerich HP, Jackson SE, Gunther, D (1996) Laser ablation inductively coupled plasma mass spectrometric transient signal data acquisition and analyte concentration calculation. J Anal At Spectrom 11: 899–904

MacIntyre RM, Mitchell JG, Dawson JB (1974) Age of the fault movements in the Tanzanian sector of the East African Rift system. Nature 247: 354–356

Mattey DP, Taylor WR, Green DH, Pillinger CT (1990) Carbon isotopic fractionation between CO_2 vapour, silicate and carbonate melts: an experimental study to 30 kbar. Contrib Mineral Petrol 104: 492–505

McGetchin TR, Besancon JR (1973) Carbonate inclusions in mantle-derived pyropes. Earth Planet Sci Lett 18: 408–410

McInnes BIA, Cameron EM (1994) Carbonated, alkaline hybridizing melts from a sub-arc environment: mantle wedge samples from the Tabar–Lihir–Tanga–Feni arc, Papua New Guinea. Earth Planet Sci Lett 122: 125–141

Meen JK (1987) Mantle metasomatism and carbonatites; an experimental study of a complex relationship. Geol Soc Am Spec Pap 215: 91–100

Minarik WG, Watson EB (1995) Interconnectivity of carbonate melt at low fraction. Earth Planet Sci Lett 133: 423–437

Norman M, Pearson N (1998) Coexisting andesitic and carbonate melts in a lherzolite xenolith from Eastern Australia. EOS Trans 79: 1004

Porcelli DR, O'Nions RK, Galer SJG, Cohen AS, Mattey DP (1992) Isotopic relationships of volatile and lithophile trace elements in continental ultramafic xenoliths. Contrib Mineral Petrol 110: 528–538

Pyle J, Haggerty SE (1994) Silicate–carbonate liquid immiscibility in upper-mantle eclogites: implications for natrosilicic and carbonatitic conjugate melts. Geochim Cosmochim Acta 58: 2997–3011

Rudnick RL, McDonough WF, Chappell BW (1993) Carbonatite metasomatism in the northern Tanzanian mantle: petrographic and geochemical characteristics. Earth Planet Sci Lett 114: 463–475

Saal AE, Hart SR, Shimizu N, Hauri EH, Layne GD (1998) Pb isotopic variability in melt inclusions from oceanic island basalts, Polynesia. Science 282: 1481–1484

Schiano P, Clocchiatti R, Shimizu N, Weis D, Mattielli N (1994) Cogenetic silica-rich and carbonate-rich melts trapped in mantle minerals in Kerguelen ultramafic xenoliths: implications for metasomatism in the oceanic upper mantle. Earth Planet Sci Lett 123: 167–178

Smith D (1987) Genesis of carbonate in pyrope from ultramafic diatremes on the Colorado Plateau, southwestern United States. Contrib Mineral Petrol 97: 389–396

Veksler IV, Petibon C, Jenner GA, Dorfman AM, Dingwell DB (1998) Trace element partitioning in immiscible silicate–carbonate liquid systems: an initial experimental study using a centrifuge autoclave. J Petrol 39: 2095–2104

Wallace ME, Green DH (1988) An experimental determination of primary carbonatite magma compositions. Nature 335: 343–346

Wendlandt RF, Harrison WJ (1979) Rare earth partitioning between immiscible carbonatite and silicate liquids and CO_2 vapor: results and implications for the formation of light rare earth-enriched rocks. Contrib Mineral Petrol 69: 409–419

Wiechert U, Ionov DA, Wedepohl KH (1997) Spinel peridotite xenoliths from Atsagin–Dush volcano, Dariganga lava plateau, Mongolia: a record of partial melting and cryptic metasomatism in the upper mantle. Contrib Mineral Petrol 126: 345–364

Woolley AR, Kempe DRC (1989) Carbonatites: nomenclature, average chemical compositions, and element distributions.

In: Bell K (ed) Carbonatites, genesis and evolution. Unwin Hyman, London, pp 1–14

Wyllie PJ, Huang W-L (1976) Carbonation and melting reactions in the system $CaO–MgO–SiO_2–CO_2$ at mantle pressures with geophysical and petrological applications. Contrib Mineral Petrol 54: 79–107

Wyllie PJ, Lee W-J (1998) Model system controls on conditions for formation of magnesiocarbonatite and calciocarbonatite magmas from the mantle. J Petrol 39: 1885–1893

Yang J, Godard G, Kienast JR, Lu Y, Sun J (1993) Ultrahigh-pressure (60 kbar) magnesite-bearing garnet peridotites from northeastern Jiangsu, China. J Geol 101: 541–554

Yaxley GM, Green DH (1996) Experimental reconstruction of sodic dolomitic carbonatite melts from metasomatized lithosphere. Contrib Mineral Petrol 124: 359–369

Yaxley GM, Crawford AJ, Green DH (1991) Evidence for carbonatite metasomatism in spinel peridotite xenoliths from western Victoria, Australia. Earth Planet Sci Lett 107: 305–317

Yaxley GM, Green DH, Kamenetsky V (1998) Carbonatite metasomatism in the southeastern Australian lithosphere. J Petrol 39: 1917–1930

Zhang RY, Liou JG (1994) Significance of magnesite paragenesis in ultrahigh-pressure metamorphic rocks Am Mineral 79: 397–400